Optical Characterization of Commonly Used Thermal Control Paints in a Simulated GEO Environment

Miles Bengtson, Jordan Maxwell
University of Colorado Boulder
Ryan Hoffmann, Russell Cooper, Stephanie Schieffer, Dale Ferguson, W. Robert Johnston
Air Force Research Laboratory, Space Vehicles Directorate
Heather Cowardin
Jacobs, NASA Johnson Space Center
Elena Plis, Daniel Engelhart
Assurance Technology Corporation

ABSTRACT

Ground- and space-based optical observations of space objects rely on knowledge about how spacecraft materials interact with light. However, this property changes as a result of materials' surface interactions with the harsh space environment. Dynamic reflectivity of spacecraft material must be taken into account to provide positive identification and improved space situational awareness (SSA). Additionally, a thorough characterization of each spacecraft material's optical properties while on orbit can be used to fine tune spacecraft surfaces for optimal thermal properties throughout a mission lifetime. This work presents an investigative study into the evolution of spectral reflectivity of commonly used spacecraft thermal control coatings manufactured by AZ Technologies under simulated geosynchronous Earth orbit (GEO) conditions. Samples were subjected to GEO-like electron fluxes, then hemispherical reflectance and bidirectional reflectance distribution functions were measured as a function of electron exposure.

1. INTRODUCTION

Astronomical reflectance spectroscopy is a maturing technique for identification and characterization of artificial space objects. This technique has been applied to identify material compositions of asteroids and other near-Earth objects, and several recent studies have demonstrated the possibilities for application to remotely characterize satellites, rocket bodies, and other artificial space objects [1-5]. Though objects in GEO are generally not resolved when observed remotely, the reflected light captured by even from a few pixels contains significant information in the spectral, polarimetric, and radiometric domains which can be leveraged for SSA purposes [6, 7]. Reflectance spectroscopy involves observation of the sunlight reflected off spacecraft surfaces via ground-based or space-based detectors over a wide-range of wavelengths but utilizing narrow-band filters for quantitative analysis. The solar spectrum is continuous in wavelength, and every material reflects (or absorbs) different wavelengths of light in a unique way. The reflection spectrum of a spacecraft will comprise features specific to the surface materials which can be used to derive the material composition within a resolved or non-resolved image.

To further maximize the value of space object spectroscopy for the SSA community, it is important to understand how the space environment causes spacecraft material properties to change. Material aging in GEO is caused by energetic particle fluxes, solar VUV light, and thermal cycling between 120-420 K [8]. Energetic electrons deposit the majority of energy to the material [9]. Energetic protons also cause damage to GEO objects; however, they have a lower average flux which varies significantly with the solar cycle and consequently this paper focuses on electron irradiation. We have previously investigated the chemical mechanisms underlying the material properties of polyimide and multi-layer insulation change with exposure to a simulated GEO space weather environment [3, 10-12]. These studies represent the first steps toward developing detailed physics-based models of the most common spacecraft materials for remote characterization purposes. This paper builds upon the previous work by applying the reflectance spectroscopy technique to a different class of spacecraft materials: white thermal control paints. Numerous studies have investigated the optical properties of thermal control coatings, seeking to understand their degradation and improve end-of-life performance [13-16]. To our knowledge, this is the first study devoted to the investigation of the reflectivity of white thermal control paints under simulated GEO conditions with the goal of developing advanced SSA techniques for on-orbit identification and remote diagnosis of spacecraft health.

The manuscript is structured as follows: Section 2 describes the details of the thermal control coatings which were tested, Section 3 outlines the material aging method applied to the samples and discusses the optical measurement system. Section 4 discusses the data analysis procedure and presents experimental evidence of optical degradation of thermal control paints under high energy electron irradiation. In Section 5, we present a color-color plot using Sloan Digital Sky Survey (SDSS) filters [17] to illustrate how ground- or space-based sensor systems could be used to remotely determine a spacecraft's material composition. Results of this work have important implications for the developing field of reflectance spectroscopy for positive characterization and identification of artificial space objects. In addition, this work is also highly relevant for satellite designers to understand the degradation of thermal paints in the space environment and to improve end-of-life satellite performance.

2. SAMPLES INVESTIGATED

Eight commonly-used white spacecraft paints were provided by AZ Technology for this study. Table 1 provides the sample ID along with the thickness, density, absorption, and emittance of each of sample investigated. Both organic and inorganic paints were studied. It is commonly known that AZ-93 consists of a zinc oxide pigment in a potassium silicate binder. The chemical formula of the pigments and binders for the other samples are proprietary to AZ technology. In addition to the paints, two samples of Mylar and two samples of Kapton were included in the experiment for comparison as the optical properties of these materials under electron bombardment have previously been studied [3, 10].

Each paint was applied to a 1-inch diameter aluminum disk substrate by the manufacturer using the same techniques that would be used if it was being applied to a rocket body. Each sample disk was mounted on an aluminum carousel with a piece of double-sided, conductive, copper tape, as shown in Figure 1. Prior to beginning the experiment, the samples were baked-out in vacuum for 48 hours at 60° C.

Table 1: Description and classification of samples under test [18, 19].

Sample		**Sample ID**	**Coating**	**Thickness (mil)**	**Density (g/cm^2)**	**Solar Absorption** (± 0.02)	**Thermal Emittance** (± 0.02)
White Paint	Inorganic	1	AZ-2170	5.0	2.2	0.15	0.90
		2	AZ-2100	4.5	2.2	0.15	0.90
		3	AZ-93	5.7	2.2	0.15	0.91
		4	AZW-LAII	7.8	2.1	0.090	0.91
		7	AZ-2000	4.0	2.2	0.25	0.88
	Organic	5	AZ-400	3.8	2.2	0.169	0.89
		6	AZJ-4020	7.5	2.4	0.15	0.88
		8	AZ-3700	1.0-2.0	2.3	0.22-0.25	0.25-0.33
Kapton-H®		9	n/a	2	1.4	≤ 0.44	≥ 0.71
		10					
Mylar		11	n/a	2	1.4	≤ 0.14	≤ 0.035
		12					

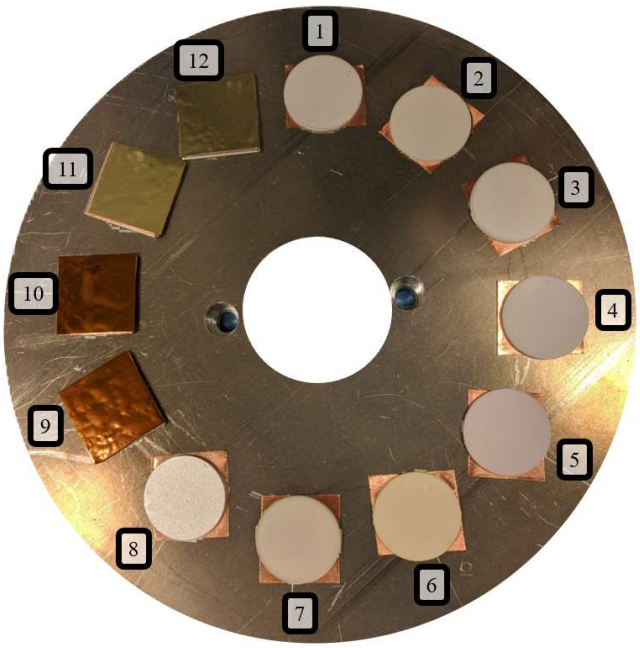

Figure 1: Carousel with mounted samples. The Faraday cup was mounted in the hole in the center of the carousel.

3. EXPERIMENTAL SETUP

The sample carousel was mounted inside the Jumbo Environmental Chamber in the Spacecraft Charging and Instrument Calibration Laboratory (SCICL) at Kirtland Air Force Base in New Mexico, USA [20]. This vacuum chamber uses a cryogenic pump to achieve vacuum levels on the order of 10^{-6} Torr. To recreate the electron radiation dose on a GEO object over a satellite lifetime, samples were bombarded with high energy (90 keV) mono-energetic electron radiation from a Kimball Physics EG8105-UD electron gun. Throughout the irradiation, the sample carousel was rotated to ensure uniform doses for all samples. A Faraday cup mounted in the center of the carousel measured the electron flux continuously to allow for accurate determination of the total fluence.

Reflectance spectra were recorded at regular intervals using an in-vacuum integrating sphere which measures hemispherical reflectance (HR). During each measurement operation, the electron beam was blanked, and the integrating sphere was moved over the sample carousel using an automated 3-D motion system. The carousel then rotated each sample in front of the integrating sphere, so a spectrum of each paint could be obtained. To minimize the stray light entering or exiting the measurement system, the integrating sphere was mounted on a ball joint/spring mechanism which presses the front of the integrating sphere flush against the surface to be measured. Due to alignment issues, the data had to be post-processed to correct for light which leaked out at the interface between the sample and the integrating sphere, as is discussed in the following section.

An ASD FieldSpec Pro spectroradiometer with a measurement range of 350-2500 nm was used to record the spectra. An HL-2000-HAS halogen lamp manufactured by Ocean Optics was used as a light source to produce high-intensity light between 400-2100 nm. At the start of each measurement cycle, white and black reference spectra were obtained in vacuum. The white spectrum, which allows the raw counts to be converted to absolute reflectance, was collected over a piece of Spectralon, a highly reflective, diffuse surface, manufactured and calibrated by LabSphere. The black spectrum, which was used to subtract the signature of the integrating sphere and detector dark current from the spectra, was taken over a piece of Acktar Spectral Black. The material works well as a black standard between 400-2500 nm. Though a calibrated sample of Acktar Black was not obtained, Acktar Black has a reflectance less than 3% over the measurement range of interest [21]. A dark image was taken with the lamp shutter closed when the integrating sphere was over the Acktar Black. The dark image was used to quantify the electronic noise inherent in the optical system, though it is not important to the analysis procedure, as the black image contains the dark current spectrum. During irradiation periods, the integrating sphere, which is housed in an aluminum casing, was parked over the Spectralon to ensure that the Spectralon, which is a dielectric, did not become charged or aged due to irradiation from the electron

source. Figure 2 shows a block diagram schematic of the experiment setup. The samples, Spectralon and Acktar Black references, and integrating sphere were located inside the chamber, whereas the halogen light source and spectroradiometer were outside the chamber. Four fiber optic cables were used (two in vacuum, two out of vacuum) along with two fiber optic feedthroughs. These elements have low attenuation over the wavelength range of interest (400-1800 nm); however, light is lost at the interfaces between each element. The optical system produces a signal-to-noise ratio greater than 2.7 in the 400-1800 nm range of interest. Figure 3 shows two pictures of the experiment inside the vacuum chamber.

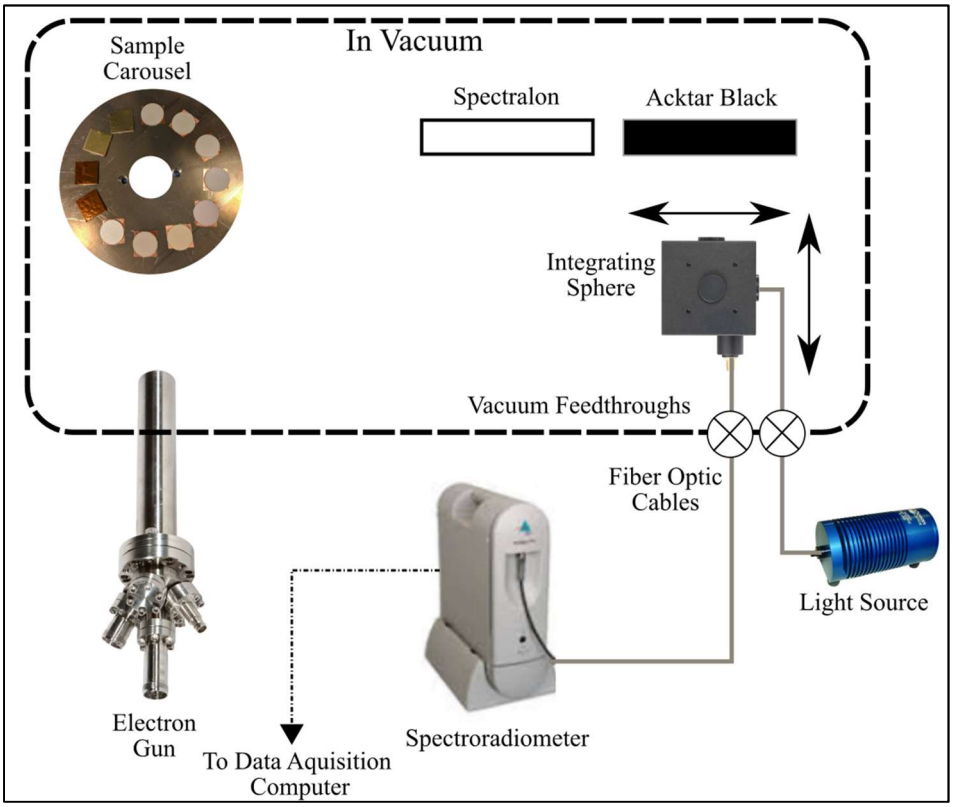

Figure 2: Block diagram of experiment.

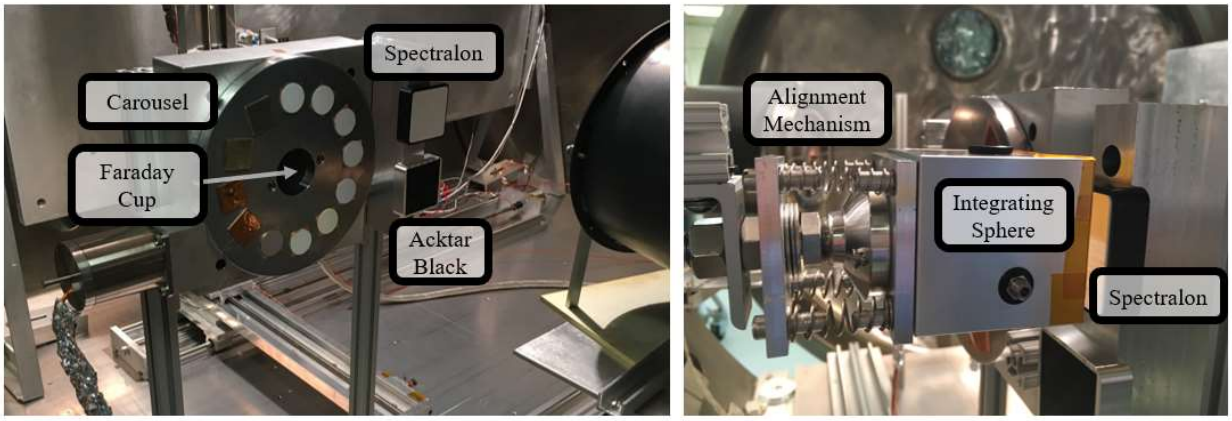

Figure 3: Experimental setup (left) and detail of the integrating sphere approaching the Spectralon sample (right). Electron gun is not pictured.

In addition to reflection spectra, the bidirectional reflection distribution functions (BRDF) of each material were measured before and after electron aging using a MiniDiff (Light Tec) handheld BRDF device and the Mini-Diff software. The measurement device measures the BRDF using collimated light (centered at 632 nm) with incidence

angles of 0°, 20°, 40°, and 60°. Although measurements in vacuum were not possible due to the nature of the device, measurements were taken after no more than 5 minutes of air exposure. Previous experiments indicate that air exposure can rapidly change the material chemistry of electron irradiated samples [22].

4. RESULTS

The following describes how corrected, absolute reflectance spectral data measurements are obtained from raw spectrometer counts. The first calculation utilizes Eq. 1 to calculate the absolute reflectance from raw spectrometer counts using the calibration materials (Spectralon and Acktar Black):

$$\frac{\frac{N_{Sample}-N_{Acktar}}{N_{Spectralon}-N_{Acktar}}}{R_{Spectralon}} \quad \text{(Eq. 1)}$$

where N represents the spectrometer counts of the indicated measurement and $R_{Spectralon}$ is the calibrated absolute reflectance of Spectralon. This method was applied to each of the samples including the eight white paints. The initial results showed a significant, non-reproducible, non-physical reduction in counts across all wavelengths during some of the measurements. We determined this to be a result of the integrating sphere not being flush to the samples, which allowed light to leak out of the measurement system, significantly reducing the total signal. The misalignment occurred at the interface between the 3D motion system and the integrating sphere. As a result, the integrating sphere remained centered over the samples, but a gap on the order of millimeters developed between the samples and integrating sphere face for some measurements. To correct for this error, the procedure described below was followed to obtain scaling factors for each of the measurements:

1. Ultraviolet-visible spectroscopy (UV/Vis) data was collected using a Perkin-Elmer Lambda 950 UV/VIS Spectrometer (0.2 – 2.5 μm) before and after the in-vacuum aging experiments to characterize the pristine and final sample spectra.
2. Pristine and aged UV/Vis spectra were compared for each material to determine features which remained constant throughout the aging process. Such features were determined for five of the twelve samples: AZ3700, Kapton (two samples), and Mylar (two samples). The five samples and the wavelengths at the peaks of the constant features (i.e., the wavelengths at which their reflectances remain constant) are given in Table 2. Though some other samples had wavelengths with constant reflectance, these wavelengths occurred in regions of the IR where the measurement noise was prohibitively large.
3. For every measurement cycle, Eq. 2 was used to determine a correction factor for each sample:
$$\alpha_i = \frac{R_{Pristine}}{R_{Aged}} \quad \text{(Eq. 2),}$$
where α_i is the correction factor for each material i, $R_{Pristine}$ is the reflectance of the pristine sample at the constant wavelength, and R_{Aged} is the reflectance of the aged sample at the constant wavelength.
4. The correction factors for each material in a given measurement cycle were very close, confirming that the observed shift in counts was caused by variations in the integrating sphere-sample alignment. The material-specific scaling factors for each measurement cycle were averaged to obtain one scaling factor for that measurement cycle. Table 3 gives the resulting scaling factors.
5. The measured reflectance for every material were multiplied by the correction factor at each measurement cycle, as shown in Eq. 3:
$$R_{Vacuum_{Corrected}} = \alpha R_{Vacuum} \quad \text{(Eq. 3)}$$

Table 2: Wavelengths used to determine scaling factors.

Sample	Wavelength used for scaling [nm]
AZ3700	875
Kapton 1	1660
Kapton 2	1660
Mylar 1	1660
Mylar 2	1660

Table 3: Electron fluence and associated correction factors used for each measurement cycle.

Measurement Cycle	Electron Fluence (10^{14} cm^{-2})	Correction Factor
1	0	1.00
2	2.046	1.00
3	3.317	1.22
4	6.305	1.30
5	11.93	1.18

Corrected spectral reflectance as a function of electron fluence (1-5 in increasing dosages) for each of the white paints are shown in Fig 4. In each panel, the solid blue line indicates the pristine spectrum which was taken before electron irradiation. Seven of the eight white paints exhibited significant changes in optical reflectance after irradiation. With the exception of AZ3700, all the paints show a large decrease in reflectance in the near-IR region. AZ2100, AZ93, AZLAII, AZ400, and AZ2000 display absorption features at wavelengths around 600 nm. The results for AZ93 are remarkably similar to those presented in [13] for ZnO paint irradiated with 70 keV electrons. This suggests that AZ93 is a ZnO based paint and also that the scaling process was successful in corrected for light lost by the integrating sphere misalignment. The results presented in [13] also show that spectra taken at the highest fluences sometimes have greater reflectances than those taken at lower fluences (though the pristine measurement always shows the greatest reflectance). Figure 4 shows that, for many of the materials, there is an initial decrease in reflectance from the pristine value with irradiation. However, after the initial decrease, the reflectance either remains relatively constant or does not monotonically decrease with additional irradiation.

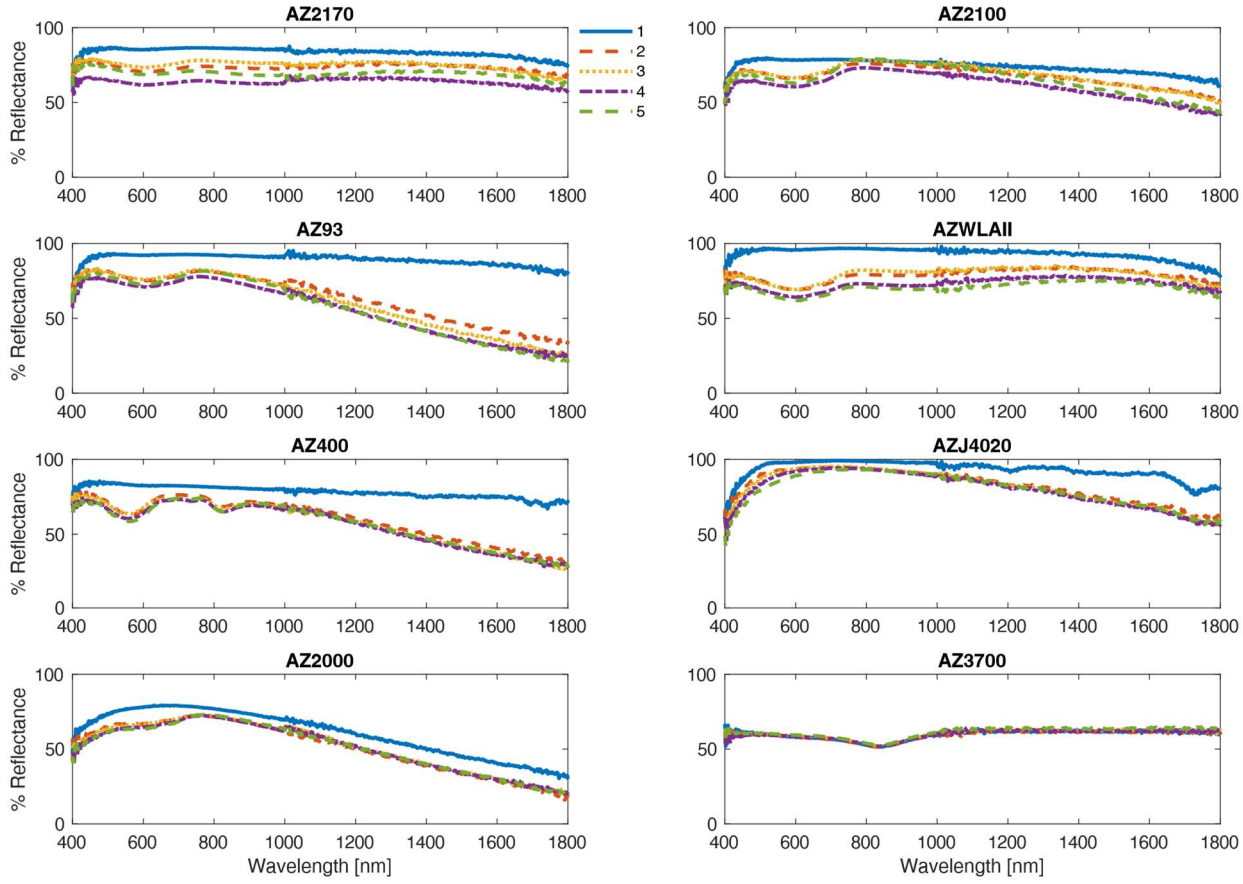

Figure 4: Spectral reflectance as a function of electron fluence for eight white paint samples. The measurements 1-5 correspond to the fluences given in Table 3.

Figure 5 shows the spectral reflectance variation of the Kapton and Mylar samples with increasing electron irradiation. The change in spectral reflectance for Kapton closely agrees with our previously published results [3].

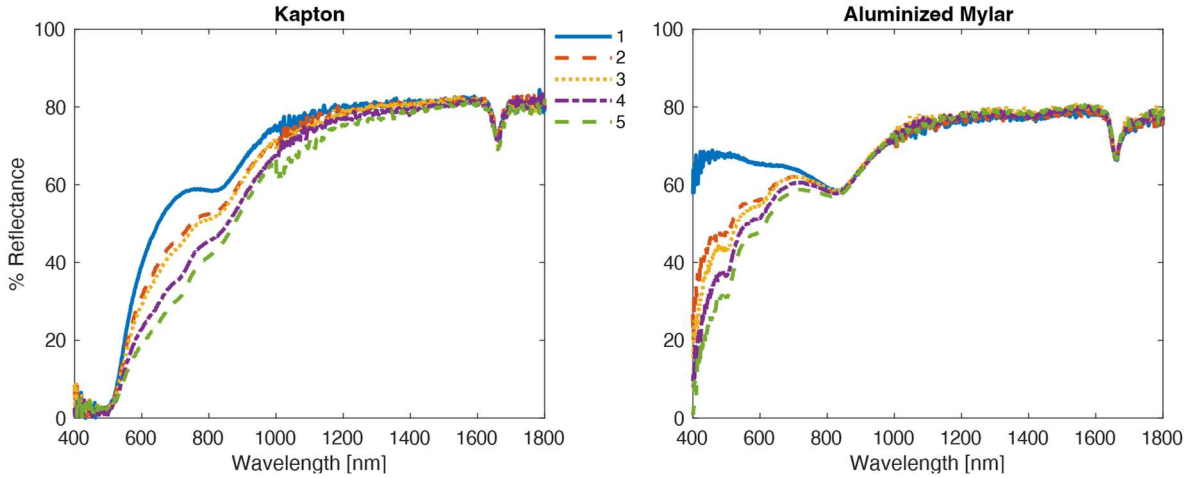

Figure 5: Spectral reflectance variation with electron fluence for Kapton and Aluminized Mylar samples. The measurements 1-5 correspond to the fluences given in Table 3.

Figure 6 shows the 0° incidence angle BRDFs of each material before and after irradiation.

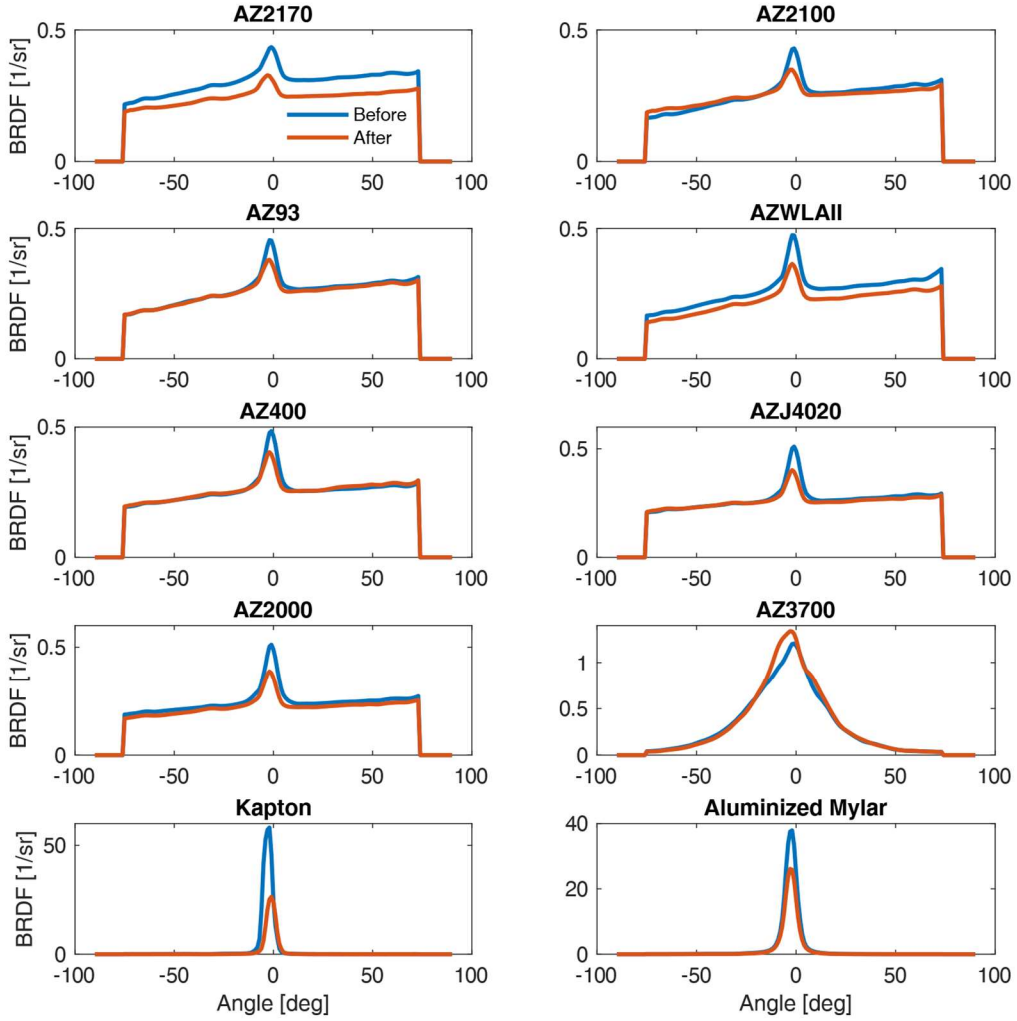

Figure 6: Pristine and aged BRDFs for each material.

5. DISCUSSION

For seven of the eight white paints, there is an overall decrease in the reflectance in addition to the spectral response. AZ3700 was the only exception; its spectral reflectance remained constant with increasing electron irradiation. There is not a notable trend between the organic (AZ-400, AZ-4020, AZ-3700) and inorganic (AZ-2170, AZ-2100, AZ-93, AZW-LAII, and AZ-2000) coatings.

To quantify what a telescope operator would detect when observing a space object coated in these materials using standard astronomic filters, color/color plots are generated using astronomical SDSS filters to show changes in spectral brightness as a function of time on orbit [17]. Figure 7 shows the difference between the brightness in the *r'* band (558-682 nm) and the *i'* band (705-835 nm). The color shift for the Kapton samples are qualitatively similar to those obtained in a previous study [3]; however, the results differ quantitatively because different types of Kapton were used. As shown in the *r'-i'* plot, the white paint and Mylar samples exhibit minor changes compared to the Kapton samples. AZ-2170, AZW-LAII, AZJ-4020 showed an overall decrease in reflectance which was more significant than the relative spectral changes. As a result, there is not a clear trend in the color change with increasing fluence for these samples. AZ-2100 and AZ-2000 experienced spectral changes around 600 nm with a smaller broad-spectrum decrease in reflectance compared to the other samples. As a result, there is a clear trend in the color-color index which matches the trend for Kapton, though the change is smaller in magnitude. AZ-2100, AZ-93, AZ-400, and AZJ-4020 experienced notably decreased reflectance in the IR region (beyond 1000 nm). By utilizing filters further into the IR, the color changes of these samples as a function of increasing fluence may appear more dramatic. Determination of such a filter set is beyond the scope of this paper. Discussion of other filter sets such as Johnson or Space Object Identification in Living Color (SILC) filters applied to satellite observations is given in [23].

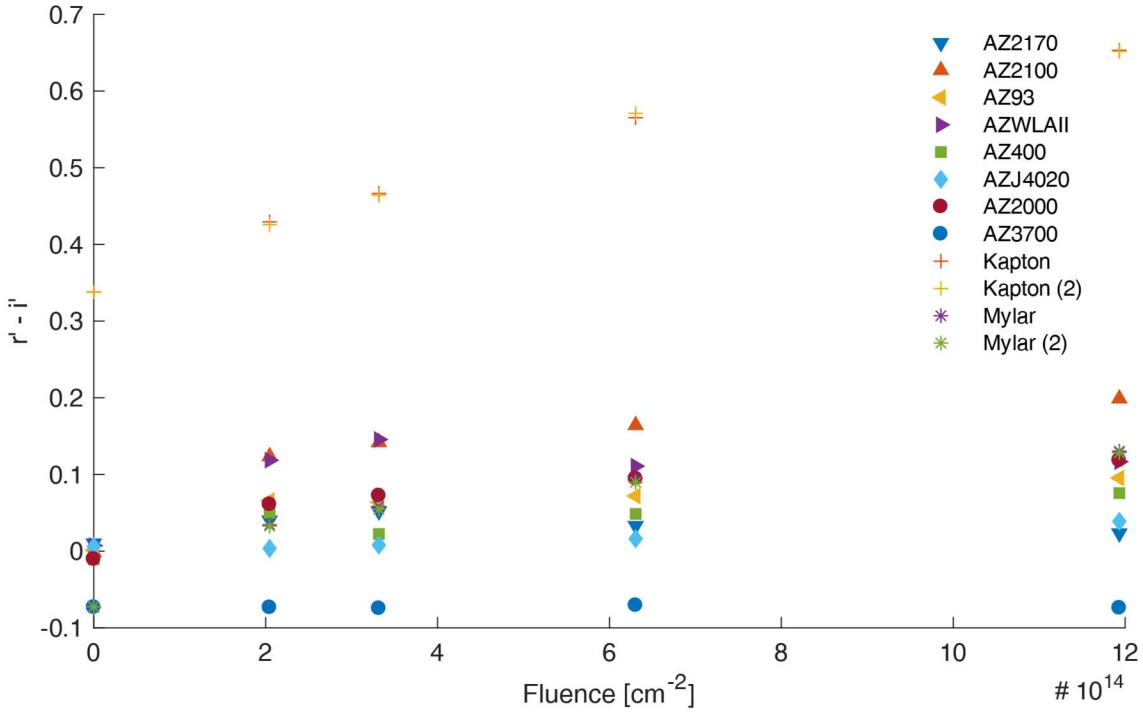

Figure 7: *r'-i'* variation with electron fluence for each material.

The normal incidence BRDF spectra of each paint and polymer sample before and after irradiation are shown in Figure 6. Comparison between pristine and aged BRDFs show an overall attenuation of the entire BRDF and especially the enhanced backscatter peak centered at 0°. Comparison of the BRDF spectra before and after irradiation revealed that no new features appeared. However, the overall signal was attenuated after irradiation with the sharp features in the distribution functions generally smoothed. Using the reflection spectra shown in Figure 4 and Figure 5, we calculated the change in absorption at 632 nm (the wavelength at which the BRDF spectra were taken) before and after irradiation and compared it to the change in the enhanced backscatter peak, as shown below in Table 4. While the radiation induced increase in optical absorption at 632 nm does not fully explain the reduced BRDF peak height, it is clearly

one factor in the observed changes. This result is a clear indication that to develop a predictive model for spacecraft spectroscopy, one must consider environmentally-induced changes both in the BRDF and reflectance/absorption spectrum of each surface material.

Table 4: Changes in BRDF peak height and absorption after irradiation (maximum fluence)

Material	BRDF Irradiated/Pristine	α (632 nm) Irradiated/Pristine
AZ2170	0.75	0.875
AZ2100	0.82	0.889
AZ93	0.83	0.867
AZWLAII	0.768	0.691
AZ400	0.833	0.881
AZJ4020	0.787	0.954
AZ2000	0.757	0.893
AZ3700	1.110	1.002
Kapton	0.453	0.597
Mylar	0.689	0.815

6. CONCLUSION

This study presents the optical effects of aging in a simulated GEO environment for various samples of thermal control white paints, Mylar, and Kapton. Although the changes in the SDSS filter *r′-i′* plots of the white paints did not show drastic differences after aging, the reflection spectra of all the samples (excepting AZ-3700) were altered dramatically. Using an optimized filter set, one could correlate the change in the sample color with fluence, allowing use of reflectance spectroscopy as a tool for characterization and identification of known and unknown GEO objects. Determination of an optimized filter set is beyond the scope of this paper and is left for future studies. Future work should also consider aging under both electron and proton irradiation to more accurately model the GEO environment, and also investigate other commonly used spacecraft surface materials. The results of this work will be important for future SSA missions to identify and mitigate threats to operational assets in the GEO environment.

7. ACKNOWLEDGEMENTS

We would like to acknowledge support from the Air Force Office of Scientific Research, Remote Sensing and Imaging Physics Portfolio (Dr. Stacy Williams; grant 17RVCOR414) and AZ Technologies Inc. for providing samples.

8. REFERENCES

[1] K. Aberkromby, K. Hamada, M. Guyote, J. Okada and E. Barker, "Remote and ground truth spectral measurement comparisons of FORMOSAT III," in *Advanced Maui Optical and Space Surveillance Technologies Conference*, Maui, USA, 2007.

[2] K. Jorgensen, Using reflectance spectroscopy to determine material type of orbital debris, Boulder: University of Colorado, 2000.

[3] D. Engelhart, R. Cooper, H. Cowardin, J. Maxwell, E. Plis, D. Ferguson, D. Barton, S. Schiefer and R. Hoffman, "Space Weathering Experiments on Spacecraft Materials," in *Advanced Maui Optical and Space Surveillance Technologies Conference*, Maui, USA, 2017.

[4] K. Abercormby, B. Buckalew, P. Abell and H. Cowardin, "Infrared Telescope Facility's Spectrograph Observations of Human-made Space Objects," in *Advanced Maui Optical and Space Surveillance Technologies Conference*, Maui, 2015.

[5] K. Aberkromby, J. Rapp, D. Bedard, P. Seitzer, T. Cardona, H. Cowardin, E. Barker and S. Lederer, "Comparisons of a Constrained Least Squares Model versus Human-in-the-loop for Spectral Unmixing to Determine Material Type for GEO Debris," in *ESA/ESOC*, Darmstadt, 2013.

[6] F. Chun, R. Tucker, E. Weld and R. Tippets, "Spectral Measurements of Geosynchronous Satellites During Glint Season," in *Advanced Maui Optical and Space Surveillance Technologies Conference*, Maui, USA, 2015.

[7] M. Polo, A. Alenin, I. Vaughn and A. Lambert, "GEO Satellite Characterization through Polarimetry using Simultaneous Observations from nearby Optical Sensors," in *Advanced Maui Optical and Space Surveillance Technologies Conference*, Maui, USA, 2016.

[8] J. Mateo-Velez, A. Sicard-Piet, D. Lazaro, V. Inguimbert, P. Sarrailh, S. Hess, V. Maget and D. Payan, "Severe Geostationary Environments: Numerical Estimation of Spacecraft Surface Charging from Flight Data," *Journal of Spacecraft and Rockets,* vol. 53, no. 2, pp. 304-316, 2016.

[9] H. Choi, J. Lee, K. Cho, Y. Kwak, I. Cho, Y. Park, Y. Kim, D. Baker, G. Reeves and D. Lee, "Analysis of GEO Spacecraft Anomalies: Space weather relationships," *Space Weather - the International Journal of Research and Applications,* vol. 9, 2011.

[10] E. Plis, D. Engelhart, D. Barton, R. Cooper, D. Ferguson and R. Hoffman, "Degradation of Polyimide Under Exposure to 90 keV Electrons," *Physica Status Solidi,* 2017.

[11] D. Engelhart, S. Humagain, S. Greenbaum, D. Ferguson, R. Cooper and R. Hoffman, "Chemical and Electrical Dynamics of Polyimide Film Damaged by Electron Radiation," *IEEE Transactions on Plasma Science,* 2017.

[12] D. Engelhart, D. Ferguson, R. Cooper and R. Hoffman, "Optical and Chemical Characterization of Polyimide in a GEO-like Environment," in *Advanced Maui Optical and Space Surveillance Technologies Conference*, Maui, USA, 2016.

[13] X. Wang, S. He and D. Yang, "Low-energy electron exposure effects on the optical properties of ZnO/K2SiO3 thermal control coatings," *Journal of Materials Research,* vol. 17, no. 7, pp. 1766-1771, 2002.

[14] C. Tonon, C. Duvignacq, G. Teyssedre and M. Dinguirard, "Degradation of the optical properties of ZnO-based thermal control coatings in simulated space environment," *Journal of Physics D: Applied Physics,* vol. 34, no. 1, p. 124, 2001.

[15] M. Mikhailov, V. Neshchimenko and S. Yuriev, "Distinctive features of the reflection spectra of radiation resistance of coatings based on ZnO powders modified by SiO2 nanoparticles," *Journal of Surface Investigation, X-ray, Synchrotron and Neutron Techniques,* vol. 8, no. 6, pp. 1315-1319, 2014.

[16] M. Dvoretskii and M. M. Mikhailov, "Thermal radiation characteristics of reflecting coatings based on zinc oxide for space systems under the conditions of the effect of earth's radiation belts," *Journal of Advanced Materials,* vol. 2, no. 1, pp. 41-49, 1995.

[17] "Sloan Digital Sky Survey," [Online]. Available: http://www.sdss.org/dr12/algorithms/ugrizvegasun/.

[18] Sheldahl, "The Red Book," [Online]. Available: http://www.sheldahl.com/sites/default/files/Documents/ShieldingMaterials/RedBook.pdf. [Accessed 2018].

[19] AZ Technology, "Paints and Coatings," [Online]. Available: http://www.aztechnology.com/products/paints.html. [Accessed 2018].

[20] R. Cooper and R. Hoffman, "Jumbo Space Environment Simulation and Spacecraft Charging Chamber Characterization," Air Force Technical Report, Albuquerque, 2015.

[21] Acktar Advanced Coatings, [Online]. Available: http://www.acktar.com/category/BlackOpticalCoating. [Accessed 2018].

[22] E. Plis, D. Engelhart, R. Cooper, D. Ferguson and R. Hoffman, "Effect of environment on charge transport properties of polyimide films damaged by high-energy electron radiation," *Journal of Vacuum Science and Technology (submitted),* 2018.

[23] T. E. W. Payne, S. A. Gregory, D. J. Sanchez, T. W. Burdullis and S. L. Storm, "Color photometry of geosynchronous satellites using the SILC filters," in *Proc. SPIE 4490, Multifrequency Electronic/Photonic Devices and Systems for Dual-Use Applications*, San Diego, 2001.